PCCP

Accepted Manuscript

ROYAL SOCIETY OF CHEMISTRY

www.rsc.org/pccp

Physical Chemistry Chemical Physics

Dynamic Article Links ►

Cite this: DOI: 10.1039/c0xx00000x

PAPER

www.rsc.org/xxxxxx

Computational Investigations on the Catalytic Mechanism of Maleate Isomerase: the Role of the Active Site Cysteine Residues

Hisham M. Dokainish, Bogdan F. Ion and James W. Gauld*

Received (in XXX, XXX) Xth XXXXXXXXX 20XX, Accepted Xth XXXXXXXXX 20XX

DOI: 10.1039/b000000x

The maleate isomerase (MI) catalysed isomerization of maleate to fumarate has been investigated using a wide range of computational modelling techniques, including small model DFT calculations, QM-cluster approach, quantum mechanical/molecular mechanical approach (QM/MM in the ONIOM formalism) and molecular dynamics simulations. Several fundamental questions regarding the mechanism were answered in detail, such as the activation and stabilization of the catalytic Cys in a rather hydrophobic active site. The two previously proposed mechanisms were considered, where either enediolate or succinyl-Cys intermediate forms. Small model calculations as well as an ONIOM-based approach suggest that an enediolate intermediate is too unstable. Furthermore, the formation of succinyl-Cys intermediate via the nucleophilic attack of $Cys76^{-}$ on the substrate C2 (as proposed experimentally) was found to be energetically unfeasible in both QM-cluster and ONIOM approaches. Instead, our results show that Cys194, upon activation via the substrate, acts as a nucleophile and Cys76 acts as an acid/base catalyst, forming a succinyl-Cys intermediate in a concerted fashion. Indeed, the calculated PA of Cys76 is always higher than that of Cys194 before or upon substrate binding in the active site. Furthermore, the mechanism proceeds via multiple steps by substrate rotation around C2–C3 with the assistance of the now negatively charged Cys76, leading to the formation of fumarate. Finally, our calculated barrier is in good agreement with experiment. These findings represent a novel mechanism in the racemase superfamily.

Introduction

For biomolecules, structure and function are often intimately inter-related. Consequently, their chemical and physical diversity is an essential factor for life as it enables them to exhibit numerous differentiated and highly specific functionalities.[1] This range of functionality arises not only from the use of dissimilar molecules but also from geometrical isomers of the same molecule.[2] For example, L-glutamate is a building block of proteins and has a role as an essential neurotransmitter in all complex living organisms.[3] Its stereoisomer D-glutamate, however, does not share these functionalities; for example, it is instead a key component in bacterial cell wall synthesis.[4] Cells can also differentiate between isomers of exogenous molecules such as therapeutic drugs, e.g., the enantiomers of thalidomide in which one is an effective treatment for morning sickness while the other causes birth defects.[5,6]

Cis-trans isomerization (CTI) is an important approach for generating geometrical isomers,[7] and is involved in many biochemical phenomena such as protein folding.[8] Such reactions require the breaking of a double bond, which typically has a high activation barrier. However, they can be chemically-facilitated by, for example, the use of metal ions, nucleophilic attack or acid/base catalysis.[8,9] Alternatively, photo-excitation can lead to isomerization via π-π^* singlet and triplet excited states.[10-12]

A number of enzymes that catalyze CTI have been examined experimentally and theoretically, revealing a wide range of mechanisms. For example, the glutathione (GSH)-dependent enzyme maleylacetoacetate isomerase, converts maleylacetoacetate to fumarylacetoacetate via transient covalent modification.[13] The related enzyme maleylpyruvate isomerase utilizes a similar mechanism.[14] In contrast, the mechanism by which retinal isomerases converts 11-trans-retinal to 11-cis-retinal proceeds via a radical intermediate.[15] The peptidyl-prolyl cis-trans isomerase family catalyzes the interconversion of cis/trans peptide bonds that involve prolyl. Notably, they have been proposed to use a variety of different mechanistic approaches including nucleophilic and proton addition.[16,17]

Asp/Glu racemase superfamily members share several structural features including a pseudosymmetrical active site-containing domain, carboxylate-containing substrate, dioxyanion hole to help stabilize the carboxylate,[18] and in most members, two catalytic cysteinyls.[4] The catalytic role of the latter two residues has been experimentally confirmed using site directed mutagenesis,[9,19,20] and two mechanisms have been proposed for their activation. In particular, in some members such as glutamate racemase (GluRs) the catalytic Cys may be activated by a conserved His and Asp residue.[21] In contrast, a previous study on proline racemase (ProRs), involving molecular dynamics (MD) simulations suggested that activation may occur via a water or the substrate itself.[18] Regardless of such differences, however, the catalytic mechanism of all members is believed to involve

formation of an enediolate intermediate.[18,22]

Maleate cis-trans Isomerase (MI) is a member of the Asp/Glu racemase superfamily found in bacteria that collectively exhibit a diverse range of functions including catalyzing the conversion of L-amino acids to D-amino acids during cell wall biosynthesis.[19,23,24] MI is a key enzyme in the metabolic degradation pathway of nicotinic acid.[25] Notably, it is utilized by many microorganisms such as *Pseudomonas, Alcaligenes, Serratia* and *Proteus* to catalyze the geometric isomerization of maleate to fumarate (Scheme 1).[6,26] The latter is an essential intermediate in the citric acid cycle.[27] In addition, it is also an important industrial target as it is involved in aspartic and L-maleic acid production.[28,29] Recently, there has also been increasing attention in using MI for degradation of tobacco waste.[30] Hence, there is great interest in gaining a better understanding of the mechanism and properties of MI and its related enzymes.[23,29,31,32]

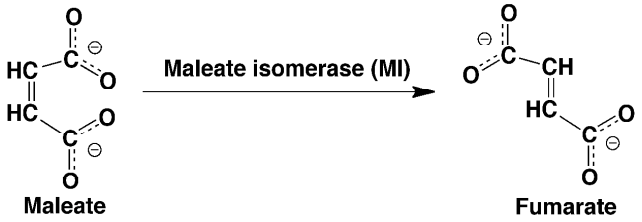

Scheme 1 Illustration of the overall isomerization reaction catalyzed by Maleate cis-trans Isomerase (MI).

Maleate cis-trans Isomerase (MI) is a cofactor-independent member of the Asp/Glu racemase superfamily.[26,33] Recently, X-ray crystal structures of both wild-type MI from *Nocardia farcinia* and the corresponding C194A mutant with a succinyl-cysteine intermediate trapped within the active site has been determined.[34] In the same study, site directed mutagenesis studies showed that mutation of Cys194 to Ala results in enzyme inactivation.[34] Furthermore, substitution of either active site cysteinyl Cys194 or Cys76 by serine reduces the rate of reaction of MI by 8000 and 1474-fold, respectively.[34] In addition, it was noted that as with other Asp/Glu racemase members several residues form a dioxyanion hole to help stabilize reaction intermediates.[9,34] However, the more hydrophobic nature of MI's active site likely results in a less effective stabilization.[34]

Based in part on these studies, two possible isomerization mechanisms have been proposed as shown in Scheme 2. Both involve an initial direct nucleophilic attack of deprotonated Cys76 (i.e., Cys76S$^-$) at the maleate substrate's C2 carbon centre. Notably, it is as yet still unclear how Cys76 is deprotonated (i.e., activated) so that it can more readily act as a nucleophile.[34] Furthermore, this nucleophilic role is distinctly different to that observed in other superfamily members such as GluR and arylmalonate decarboxylase (AMD) in which the active site cysteinyls act as acids and/or bases and do not form a covalent enzyme-substrate complex.[18,35] Importantly, in one pathway (**A**) this occurs with concomitant transfer of the Cys194 thiol proton onto the substrate's C3 carbon centre to form a succinyl-cysteine-type intermediate (Scheme 2A). It is important to mention that this intermediate has been observed using X-ray crystallography in the C194A mutant structure at high resolution and it was also confirmed using mass spectroscopy.[34] In the alternate pathway, however, Cys194 acts simply as a hydrogen bond donor to one of the substrate carboxylates throughout the mechanism, stabilizing its anionic charge (Scheme 2B). That is, pathway **B** proceeds via an enediolate-type intermediate. Despite these differences, the next step in both proposed mechanisms is rotation around the newly formed C2–C3 single bond to give a fumarate-like structure. In the succinyl-Cys pathway (Scheme 2A), the Cys76S–C2 bond dissociates concomitantly with deprotonation of -C3H$_2$- by Cys194S$^-$, thus forming fumarate with regeneration of a neutral Cys194SH. In contrast, in the enediolate pathway (Scheme 2B), cleavage of the Cys76S–C2 bond leads directly to formation of fumarate.

Computational chemistry has been shown to provide detailed insights into biological systems, and in particular, enzymatic mechanisms.[36-39] In this present study, density functional theory-based QM-cluster and ONIOM QM/MM methods have been used to investigate the initial substrate-bound active site complex and protonation states of key residues, as well as the catalytic mechanism of Maleate cis-trans Isomerase (MI).

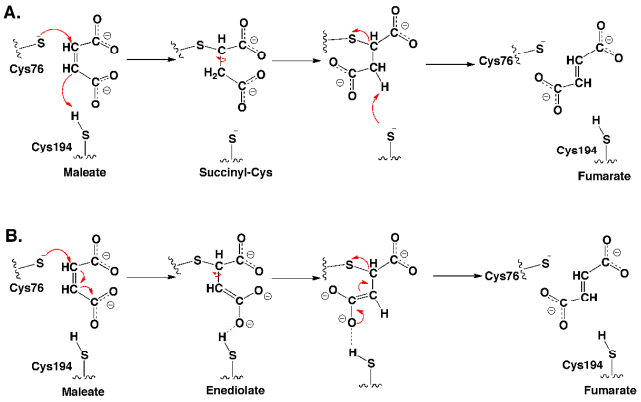

Scheme 2 Proposed mechanisms for the maleate/fumarate isomerization reaction catalyzed by MI via an (**A**) succinyl-Cys or (**B**) enediolate intermediate.[34]

Computational Methods

All docking and molecular dynamics simulations were performed using the Molecular Operating Environment (MOE) program,[40] while all QM-cluster and ONIOM QM/MM calculations were performed using the Gaussian 03[41] and 09[42] suite of programs. The density functional theory method B3LYP, a combination of Becke's three parameter exchange functional[43] and Lee, Yang and Parr's correlation functional[44] as implemented in the Gaussian programs, was the QM method used in the present calculations.

DFT-Small Model Studies

A series of initial studies were done in order to help determine an appropriate basis set to use in the larger studies (see below), and to examine the effects of the environment's polarity on the protonation state and properties of the substrate, mechanistic intermediates and product. More specifically, optimized

geometries were obtained of maleic acid, its mono- and di-anionic deprotonated derivatives, succinate and succinyl-methylthiol using the B3LYP method in combination with basis sets ranging from 6-31G(d) to 6-311+G(2df,p). Effects of a polar environment were included by use of the integral equation formalism polarizable continuum model (IEF-PCM) as implemented in Gaussian.[41,42] In particular, dielectric constants (ε) of 4 and 10 were used to model a protein environment as previously suggested,[45,46] while ε=78.39 was used to model an aqueous environment.

QM-Cluster Studies

All structures were optimized at the B3LYP/6-31G(d,p) level of theory. Relative energies were obtained via single points at the B3LYP/6-311+G(2df,p) level of theory on the optimized structures with the inclusion of the corresponding solvation correction obtained at the IEF-PCM (ε=4.0)-B3LYP/6-31G(d,p) level of theory. Frequency calculations were used to characterize transition structures as first-order saddle-points.

A suitable chemical model was derived using the X-ray crystal structure of *Nocardia farcinia,* NfMI (PDB ID: 2XEC).[34] Specifically, dianionic maleate was docked into the active site of NfMI; all residues within 10 Å of the catalytic cysteine (Cys76) being considered as the active site. In the above crystal structure the R-group of Cys76 points away from the active site pocket and therefore was manually reoriented prior to docking and MD simulations. Docking was performed using the London dG scoring function followed by optimization of the top 100 generated structures using a force field refinement method using AMBER99. The best 30 scoring structures were then examined visually to choose the most suitable starting structure for further calculations. The active site of the chosen structure was then solvated up to 10 Å from the substrate. The solvated enzyme-substrate complex was then allowed to thermally relax by performing an MD simulation for 1 ns with a time step of 2 fs as has been previously used.[47,48] A cluster analysis was then performed based on the distance between the sulfur of Cys76 and maleate's -C2H_2- carbon in order to obtain an average structure, which was then optimized using the AMBER99 force field.[49] From this optimized structure, the active site-bound substrate model shown in Scheme 3 was obtained for use in the QM-cluster studies. In particular, it included appropriately truncated models of Cys76, Cys194, Val78 and Gln196 as they are known or have been suggested to be catalytically important.[34] In addition, the R-groups of Tyr133, Asn14, and Asn163 were included as they directly interact with the substrate, e.g., via hydrogen bonding. Finally, Leu77 and Val195, both modelled as alanyls, were also included. As is common practice[50] when using QM-cluster models, in order to maintain the integrity of the model, a minimum number of atoms, remote from the reactive region, were kept fixed at their MM optimized coordinates and are highlighted in red in Scheme 3.

QM/MM Studies

The hybrid quantum mechanics/molecular mechanics (QM/MM) method as implemented in the ONIOM formalism in Gaussian 09[42] was used for all QM/MM calculations.[51] The reactive region, high (QM)-layer, was described using the same level of theory and basis set size as per the above QM-cluster approach, B3LYP/6-31G(d,p). The rest of the chemical model, the low (MM)-layer, was described using the AMBER96 MM force field. Relative energies were obtained via single points at the ONIOM(B3LYP/6-311+G(2df,p):AMBER96) level of theory on the above optimized structures.

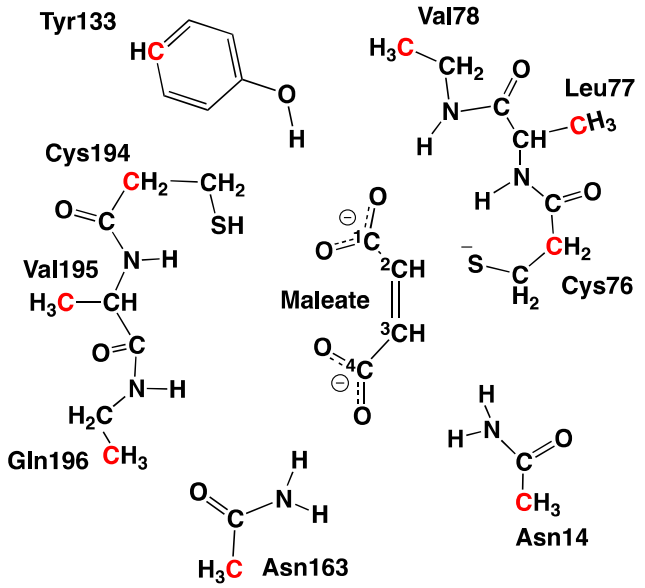

Scheme 3 The active site-bound substrate chemical model of NfMI used for the QM-cluster studies (atoms fixed at their MM optimized coordinates are highlighted in red and atom numbering used for Maleate carbons is also shown).

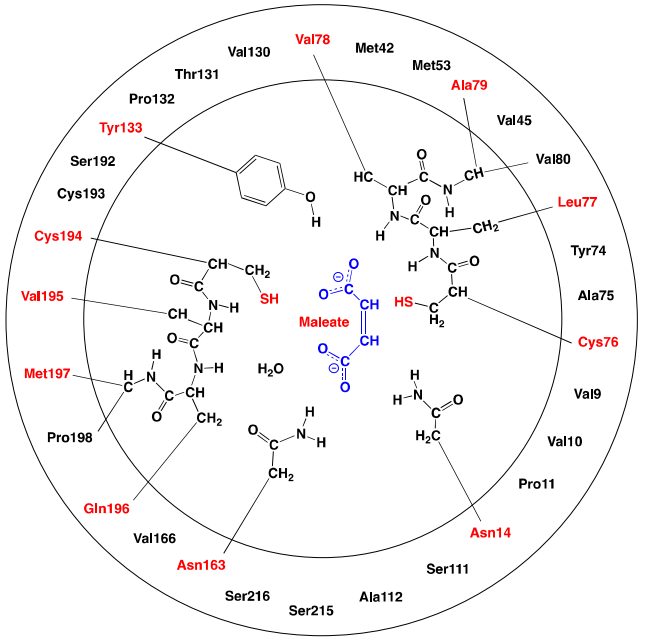

Scheme 4 Schematic illustration of the chemical model, derived from the X-ray crystal structure PDB ID: 2XED, used in the ONIOM QM/MM calculations. The inner circle represents the high (QM)-layer while the outer represents the low (MM)-layer.

A suitable chemical model for use in the QM/MM calculations was obtained from the X-Ray crystal structure of the Cys194Ala NfMI mutant enzyme with a covalently active site-bound succinyl-cysteine intermediate (PDB ID: 2XED).[34] A wild-type Michaelis complex was generated by mutating Ala194 to Cys and cleaving the enzyme-substrate covalent bond. The structure was then minimized using the AMBER99 force field. The resulting minimized structure was then truncated to include all residues within 15 Å of the substrate and is shown in Scheme 4. Within this, the QM-layer was chosen to contain all residues previously used in the QM-cluster chemical model as well as the Gln196–Met197 and Val78–Ala79 peptide bonds. All other residues were placed in the MM-layer. In order to help maintain the model's integrity, and since a large QM-layer was selected, most MM-layer atoms were held fixed at their minimized (see above) positions.[52] The QM-cluster and QM/MM optimized reactive complexes (RCs) were compared to verify consistency in their structures. Notably, their RMSDs were determined to have only quite negligible differences. In addition, the QM/MM optimized succinyl-Cys intermediate was compared to the corresponding chemical region of the crystallized intermediate (i.e., PDB ID: 2XED)[34] and found to have minor RMSDs of just 0.29 Å.

Results and Discussion

DFT-small model studies on isomerization

As noted in the Introduction, both proposed mechanisms involve nucleophilic attack of a cysteinyl thiolate at the C2/C3 position of dianionic maleate.[34] However, one proceeds via a succinyl-Cys and the other an enediolate intermediate. The former occurs with protonation of the adjacent =CH- while the latter does not (see Scheme 2). To help obtain additional insights into factors that may influence maleate to fumarate isomerization, a series of DFT-small model studies were performed. Specifically, we considered formation of these intermediates for all 3 possible ionization states of the substrate; di- (the most common form in aqueous solution)[53] and monoanionic maleate, and neutral maleic acid (Scheme 5). The HOMO and LUMO of each species was also determined, where those of maleate are shown in Figure 1.

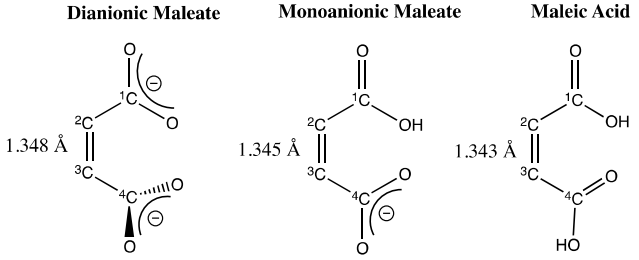

Scheme 5 Schematic illustration of the gas-phase optimized structures of the 3 possible substrate states (∠C1-C2-C3-C4 = 0.0º in each).

The gas-phase optimized structure of dianionic maleate has a ∠C1-C2-C3-C4 dihedral angle (ϕ) of 0.0º with the two carboxylates almost perpendicular to each other (Supporting Information: Table S1). The C3–C4 bond (1.543 Å) is slightly elongated with respect to C1–C2 (1.537 Å) as the HOMO lies mainly on the C1 carboxylate which lies more in the plane of the carbon backbone. Notably, C2 has only a small contribution to the HOMO orbital while to the LUMO it makes the largest contribution (Figure 1). Thus, it would be expected to be the carbon centre most susceptible to nucleophilic attack as has been proposed.[34] Increasing the polarity of the environment to 4.0 and 10.0, values commonly used to model the internal environment of a protein, the HOMO and LUMO of maleate had negligible change. It is noted that decreasing the charge in maleate via sequential protonation of the carboxylates has only quite minor effects (-0.003 and -0.002 Å respectively) on the C2=C3 bond length. Notably, however, the carboxylate/carboxylic groups now lie more in the plane of the carbon backbone (see Scheme 5).

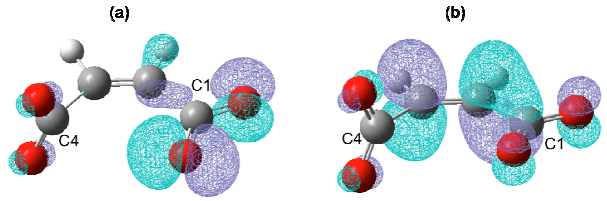

Figure 1 The (a) HOMO and (b) LUMO of dianionic maleate in the gas-phase (ε = 1).

For maleate and monoanionic maleate, nucleophilic attack of a methylthiolate (CH_3S^-) at C2 without concomitant protonation of C3 does not give a stable species for all environmental polarities (ε values) considered (ε = 1.0, 4.0, 10.0 and 78.39 (water)). Specifically, formation of an enediolate is unstable with respect to dissociation of the S–C2 bond. The same occurs for monoanionic maleate when CH_3S^- attacks at C3 (C3C4COOH) instead of C2.

In contrast, for maleic acid nucleophilic attack of CH_3S^- at C2 gives a stable enediolate structure. This occurs with marked lengthening in the C2–C3 bond from 1.343 to 1.471 Å, respectively. Simultaneously, a significant increase in the ∠C1-C2-C3-C4 angle (ϕ) occurs from 0.0º to 57.6º, respectively. Furthermore, such changes are observed for all values of ε; i.e., regardless of the environments polarity.

A stable succinyl-cysteinyl type intermediate was obtained for all 3 ionization states of the substrate. However, its nature was sensitive to the environment and the ionization state of the substrate. For example, for dianionic maleate, gas-phase formation of such an intermediate occurred with significant increases in both the C2–C3 bond length from 1.348 to 1.534 Å, and the dihedral ϕ from 0.0º to 159.7°. However, as ε was increased to 4.0, 10.0 and higher, the magnitude of rotation decreased. In contrast, for maleic acid ϕ in the resulting intermediate was reasonably consistent at approximately 60.0° for all values of ε.

Thus, it appears that both the ionization state of the substrate and the polarity of the environment can have significant effects on the stability and nature of possible mechanistic intermediates.

The ionization states of Cys76, Cys194 and the substrate

As described in the Introduction, in both proposed mechanisms, Cys76 acts as the nucleophile while Cys194 acts as a proton or hydrogen bond donor.[34] In order for Cys76 to act as a more effective nucleophile it must be deprotonated, as assumed in the mechanisms.[34] Knowing the likely initial ionization state of both active site cysteinyl residues is central for understanding their roles and the preferred reaction pathway. Consequently, the proton affinities (PAs) of the Cys76S$^-$ and Cys194S$^-$ thiolates within the various possible ionization states of the apo-enzyme and substrate-bound active site were examined using the present QM/MM models. The results obtained are shown in Figure 2.

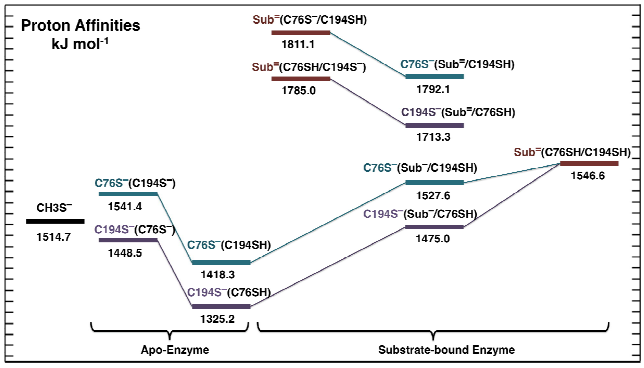

Figure 2 The calculated proton affinities (see Computational Methods) of C76S$^-$ and C194S$^-$ before and after substrate binding, and the PA of the substrate in the active site.

The proton affinity (PA) of methylthiolate (model for deprotonated cysteine) in aqueous solution is calculated to be 1514.7 kJ mol^{-1} at the present level of theory (see Computational Methods). For the active site cysteinyl thiolates (i.e., C76S$^-$ and C194S$^-$), their PAs were first calculated within the apo-enzyme active site for both possible scenarios; where the other cysteinyl is (i) anionic or (ii) neutral. For the first case the PA of C76S$^-$ is 1541.4 kJ mol^{-1} while that of C194S$^-$ is 1448.5 kJ mol^{-1}. That is, the PA of C76S$^-$ has increased while that of C194S$^-$ has decreased compared to CH_3S^- in aqueous solution. In contrast, in the case where the other cysteinyl is kept neutral the PAs of both C76S$^-$ and C194S$^-$ decrease significantly to 1418.3 and 1325.2 kJ mol^{-1}, respectively. Interestingly, in both scenarios the PA of C194S$^-$ is lowest. This may reflect the fact that as seen in the X-ray crystal structure (PDB ID: 2XED),[34] C194 is surrounded by more possible hydrogen bond donors than C76, thus any anionic charge on the former is likely to be better stabilized.

From Figure 2 it can be seen that upon binding the dianionic substrate (Sub$^=$), the proton affinity of both C76 and C194 has increased markedly from their corresponding values in all possible apo-enzyme active sites. In contrast, in all substrate-bound active sites containing one or more neutral cysteinyls, the PA of Sub$^=$ has decreased from its calculated value in aqueous solution (1877.3 kJ mol^{-1}; not shown). Importantly, however, despite these decreases, in those cases where only one of the cysteinyls is neutral, the PA of Sub$^=$ remains higher than that of the ionized cysteinyl. For instance, when C194 is neutral the PA of Sub$^=$ is 1811.1 kJ mol^{-1} while that of C76S$^-$ is 19.0 kJ mol^{-1} lower at 1792.1 kJ mol^{-1}. Similarly, when C76 is neutral, the decreased PA of Sub$^=$ (1785.0 kJ mol^{-1}) is still 71.7 kJ mol^{-1} higher than that of C194S$^-$ (1713.3 kJ mol^{-1}). Thus, in either system Sub$^=$ will be preferentially protonated over the ionized active site cysteinyl.

Indeed, the proton affinity of Sub$^=$ when both cysteinyls are neutral is 1546.6 kJ mol^{-1}, while that of the ionized cysteinyl in C76S$^-$/Sub$^-$/C194SH and C76SH/Sub$^-$/C194S$^-$ is 1527.7 and 1475.0 kJ mol^{-1}, respectively. It is noted that in the latter system the PA of C194S$^-$ is also lower than that of methylthiolate in aqueous solution.

These results thus suggest that the substrate-bound active site prefers to exist as having a monoanionic maleate and ionized Cys194 (i.e., C194S$^-$), but a neutral Cys76 (i.e., C76SH). This further suggests that the substrate itself may be able to play a role in activating an active site cysteinyl, specifically Cys194, to be the required nucleophile, while Cys76 may instead act as the proton or hydrogen bond donor.

Cys76-pathway: mechanism with Cys76 as the nucleophile

In both of the experimentally proposed mechanisms the thiol of Cys76 is deprotonated and acts as a nucleophile to attack the C2 position of dianionic maleate, while Cys194 is neutral. Such possible catalytic mechanisms were thus considered using a QM-cluster approach. The potential energy surface (PES) obtained is shown in Figure 3 while the corresponding optimized stationary point structures, with selected distances, are shown in Scheme 6.

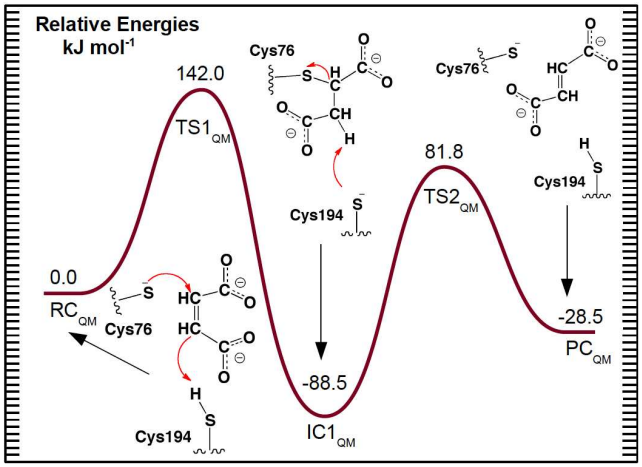

Figure 3 PES obtained using a QM-cluster approach (see Computational Methods) of the catalytic mechanism of MI in which Cys76 acts as a nucleophile.

In the optimized structure of the reactant complex, **RC$_{QM}$**, the substrate's carboxylates are each stabilized by multiple hydrogen bonds. More specifically, -C1OO$^-$ forms hydrogen bonds with the R-groups of Cys194 and Tyr133, and the backbone –NH– moieties of Leu77 and Val95. The -C4OO$^-$ carboxylate, in contrast, is stabilized by only three hydrogen bonds formed with the R-groups of Asn14 and Asn163, and the backbone –NH– of Gln196. Meanwhile, the Cys76S$^-$ forms just a single hydrogen

bond with the backbone –NH–of Val78.

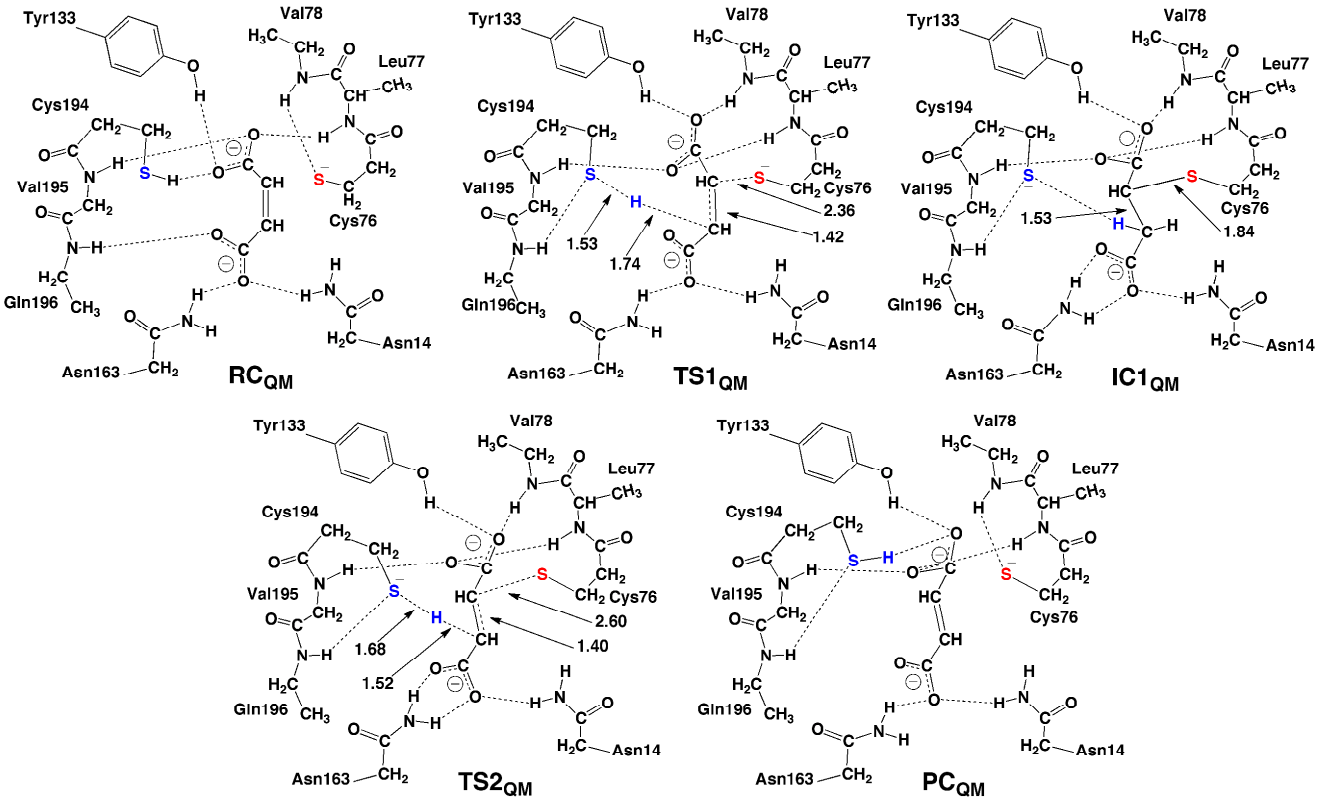

Scheme 6 Schematic illustration of the optimized structures obtained using a QM-cluster approach (see Computational Methods) for the mechanism in which Cys76 acts as nucleophile.

Using the QM-cluster approach no mechanism involving an enediolate-intermediate could be characterized. However, an alternate possible pathway involving a succinyl-Cys type intermediate was obtained. The latter begins with nucleophilic attack of the Cys76S$^-$ at the substrate's C2 center with a concomitant proton transfer from the thiol of Cys194 onto C3. This step occurs via **TS1$_{QM}$** with a markedly high relative energy barrier of 142.0 kJ mol^{-1}. In the optimized structure of **TS1$_{QM}$** (Scheme 6) the Cys76S···C distance has shortened considerably to 2.36 Å while the C3···H···SCys194 distances are 1.74 and 1.53 Å, respectively. These distances further illustrate the concomitant formation of the Cys76S—C2 bond and proton transfer from Cys194. Notably, during formation of the succinyl-Cys intermediate the ∠C1-C2-C3-C4 (ϕ) increases from 1.1° to 68.0° while the C2—C3 bond has lengthened to 1.42 Å; it now has significantly reduced double bond character. That is, **IC1$_{QM}$** resembles more a fumarate-like structure.

The resulting intermediate (**IC1$_{QM}$**) formed lies 88.5 kJ mol^{-1} lower in energy than **RC$_{QM}$**. The dihedral angle ϕ has significantly increased to 210.8 (-149.2)° while the C2—C3 bond has lengthened to 1.53 Å, i.e., is now essentially a single bond with a *trans*-like orientation of the substrate's carbon backbone. The hydrogen bond network between the substrate and active site residues is generally retained, with only some minor differences. For example the Gln196 –NH– backbone now hydrogen bonds to the thiolate of Cys76 instead of the substrates' –C4OO$^-$ group.

In the next and final step the Cys76S–C2 bond is cleaved while concomitantly the -C3H$_2$- moiety transfers a proton onto the Cys194S$^-$ thiolate. This concerted step proceeds via **TS2$_{QM}$** with a barrier of 81.8 kJ mol^{-1} with respect to **RC$_{QM}$**; 160.3 kJ mol^{-1} with respect to **IC1$_{QM}$**. That is neither step 1 or 2 are likely to be enzymatically feasible.[54,55] In **TS2$_{QM}$**, the Cys76S···C2 bond has elongated to 2.60 Å; while the Cys194S···H···C3 distances are 1.68 and 1.52 Å, respectively. As a result the C2—C3 bond now has regained some double bond character. Furthermore, the dihedral angle ϕ is now 182.9°. The product complex (**PC$_{QM}$**) lies 28.5 kJ mol^{-1} lower in energy than **RC$_{QM}$**. Notably, the C2—C3 bond is now formally a double bond with a distance of 1.34 Å while ϕ has increased slightly to 191.9°.

It is noted that the corresponding "succinyl-Cys" mechanism in which the proton transfers involving Cys194 occurred via a H$_2$O moiety was also examined. However, the relative energies with respect to **RC$_{QM}$** of **TS1$_{QM}$** and **TS2$_{QM}$** increased significantly to 123.0 and 193.9 kJ mol^{-1}, respectively.

An ONIOM(QM/MM) approach (see Computational Methods) was then used to further examine possible mechanisms in which Cys76 may act as the nucleophile. In particular, mechanisms in which Cys76 and Cys194 may initially be neutral, as suggested by the above PA calculations, were considered. The PES obtained is shown in Figure 4 while the corresponding optimized structures, with selected distances, are shown in Scheme 7.

Again, in the reactant complex the –C1OO$^-$ carboxylate is

stabilized via multiple strong hydrogen bonds with the side chain hydroxyl of Tyr133 and the backbone –NH– functionalities of Ala79, Leu77 and Val195. Similarly, the -C4OO$^-$ group is again stabilized via three strong hydrogen bonds with the side chains of Asn14 and Asn163, and the backbone–NH– of Gln196. It is noted that the thiol of Cys194 forms a weak hydrogen bond with –C1OO$^-$; r(SH···O) = 2.52 Å.

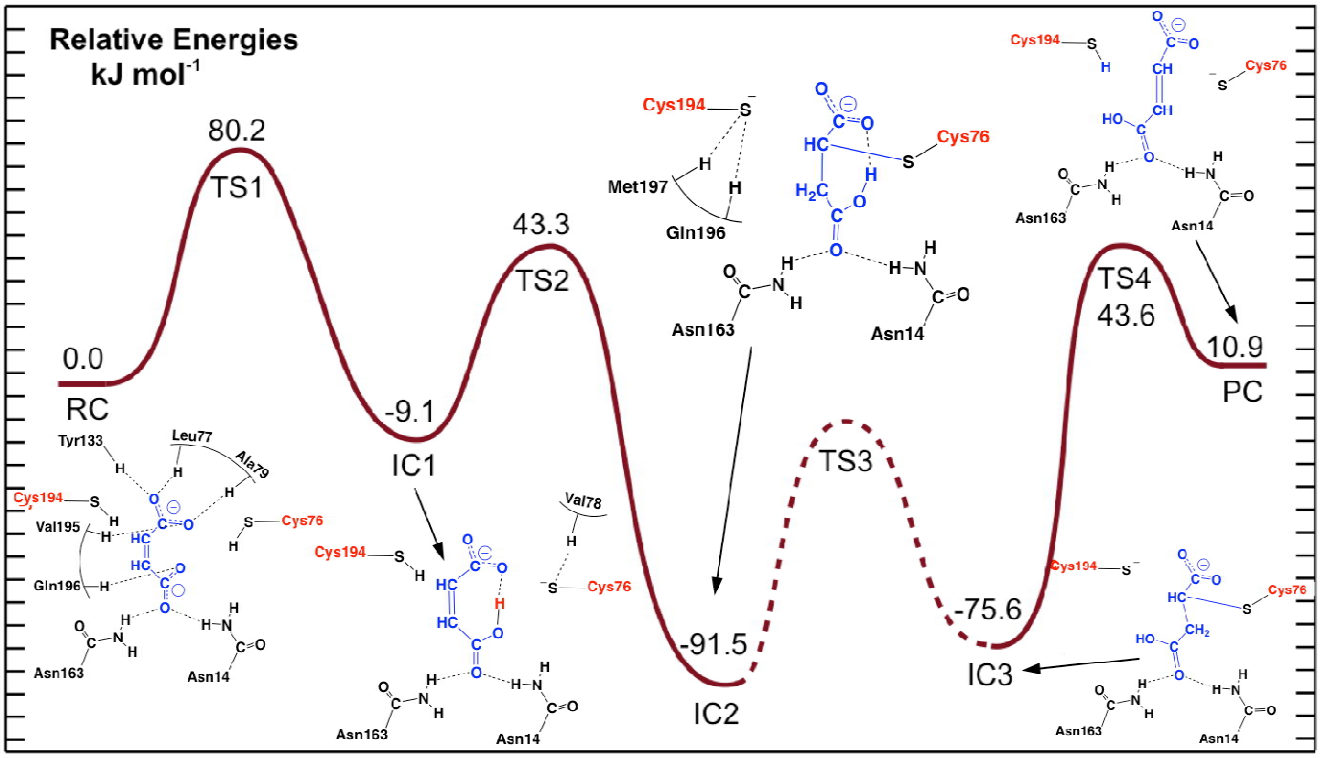

Figure 4 PES obtained using an ONIOM(QM/MM) approach (see Computational Methods) of the catalytic mechanism of MI in which Cys76 acts as a nucleophile.

As noted, Cys76SH is proposed to act the nucleophile after it has been activated, i.e., deprotonated. Unfortunately, Cys76 is situated in a hydrophobic region with no suitable candidate base residue to cause its activation. However, an alternate possibility is that the substrate may be able to facilitate such a process due to its carboxylates. Indeed, the PA calculations described above suggest that the substrate may have a suitably high-enough PA compared to Cys76SH.

In **RC**, the Cys76SH proton is 2.85 and 3.70 Å from the nearest oxygen of the –C1OO$^-$ and –C4OO$^-$ groups, respectively Table S2). The first step of the overall mechanism is transfer of the thiol proton of Cys76 via the –C1OO$^-$ moiety onto the –C4OO$^-$ group. This occurs via **TS1** with a barrier of 80.2 kJ mol^{-1} with respect to **RC** (Figure 4). In **TS1** (Scheme 7) the proton being transferred is essentially on the –C1OO$^-$ group; r(C1OO$^-$···H$^+$) = 1.05 Å. Simultaneously, however, it lies about midway between the Cys76 thiolate sulfur and the nearest oxygen of the –C4OO$^-$ moiety with distances of 2.31 and 2.15 Å, respectively (see Scheme 7). It is noted that no intermediate was obtained with the Cys76SH proton on the –C1OO$^-$ group. This may reflect that this carboxylate already makes stronger and more hydrogen bonds with active site residues than the –C4OO$^-$ group. Thus, the –C1OO$^-$ group's anionic character is better stabilized than that of the –C4OO$^-$ group. The Cys76S$^-$ thiolate now appears suitably positioned to attack C2 (Scheme 7).

In the resulting intermediate formed, **IC1**, the proton from Cys76SH has been transferred fully to the –C4OO$^-$ group. That is, the substrate is now a monoanionic maleate with a neutral Cys194. Meanwhile, the anionic Cys76S$^-$ forms a single weak hydrogen bond (2.57 Å) with the backbone –NH- of Val78. More importantly the Cys76S···C2 distance has shortened to 2.75 Å while the C2–C3 bond has elongated from 1.35 to 1.37 Å. **IC1** lies lower in energy than **RC** by just 9.1 kJ mol^{-1}.

As suggested by the DFT-small model studies (see above), a stable enediolate intermediate could not be obtained within the active site using the QM/MM model. Rather, the next step is nucleophilic attack of the thiolate of Cys76S$^-$ at the C2 carbon centre of the substrate. Concomitantly, the thiol of Cys194 transfers its proton onto the substrate's adjacent C3 center. This concerted step proceeds via **TS2** at a cost of 52.4 kJ mol^{-1} with respect to **IC1**. This is illustrated by the fact that in the optimized structure of **TS2** the Cys76S···C2 distance has shortened significantly to 1.96 Å. Meanwhile, the Cys194SH proton now lies between the Cys194 sulfur and C3 with distances of 1.51 and 1.80 Å, respectively.

The resulting succinyl-Cys intermediate formed, **IC2**, lies significantly lower in energy than **RC** by 91.5 kJ mol^{-1}. Also, the C2–C3 bond distance is now 1.54 Å. Notably, it corresponds to the crystallographically obtained "intermediate" in a Cys194Ala mutant MI enzyme.[34]

The next step is likely rotation about the C2–C3 bond (1.52 Å) to give an enzyme-bound fumarate-like intermediate **IC3**. Such a species similarly lies considerably lower in energy than **RC** by 75.6 kJ mol^{-1}. Unfortunately, no TS (**TS3**) for such a rotation could be optimized at the present level of theory. However, the barrier is expected to be feasible as observed in the Cys194-pathway discussed below (see Figure 5).

The subsequent and final step is then formation of the product complex **PC**; an active site-bound fumarate. This concerted step, involving both cleavage of the C2—SCys76 bond and a proton transfer from the substrate's -C3H2- group to Cys194, occurs via **TS4** at a cost of 119.2 kJ mol^{-1} with respect to **IC3**. Notably, the energy difference between **IC2** and **TS4** is 135.1 kJ mol^{-1}; which has been suggested to be thermodynamically greater than that which is enzymatically feasible.[54,55] This also represents the largest difference between any minimum and TS along this possible mechanism, and is likely the rate limiting step for such a mechanism. The apparent considerable energy required for **IC2** to either proceed to product or back to reactant (requires 171.7 kJ mol^{-1}) may provide insights into the ability of experimentalists to obtain an X-ray crystal structure of such an intermediate in a Cys194Ala mutant enzyme. Notably, the detection of the succinyl-Cys in C194A suggests the presence of an alternate proton-transferring agent that helps stabilize the intermediate. However, the absence of a suitable mechanistic base (i.e., loss of Cys194S^{-}) does not allow for product formation.

The final product complex, **PC**, lies slightly higher in energy than **RC** by 10.9 kJ mol^{-1}, indicating that the overall mechanism is endothermic. The C2–C3 double bond is 1.37 Å, further indicating the formation of the fumarate product.

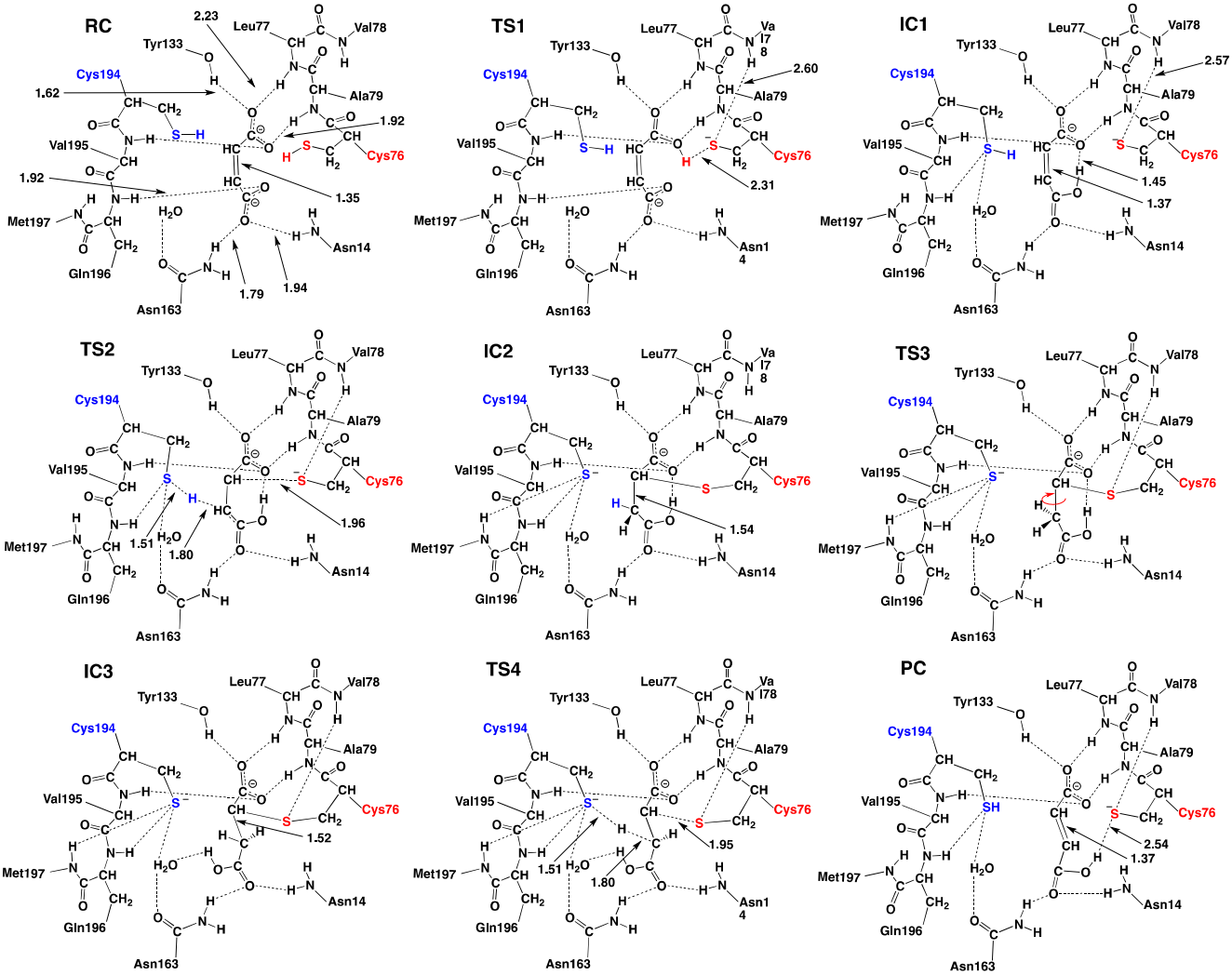

Scheme 7 Schematic illustration of optimized structures obtained using an ONIOM(QM/MM) approach (see Computational Methods) for the mechanism in which Cys76 acts as nucleophile.

.

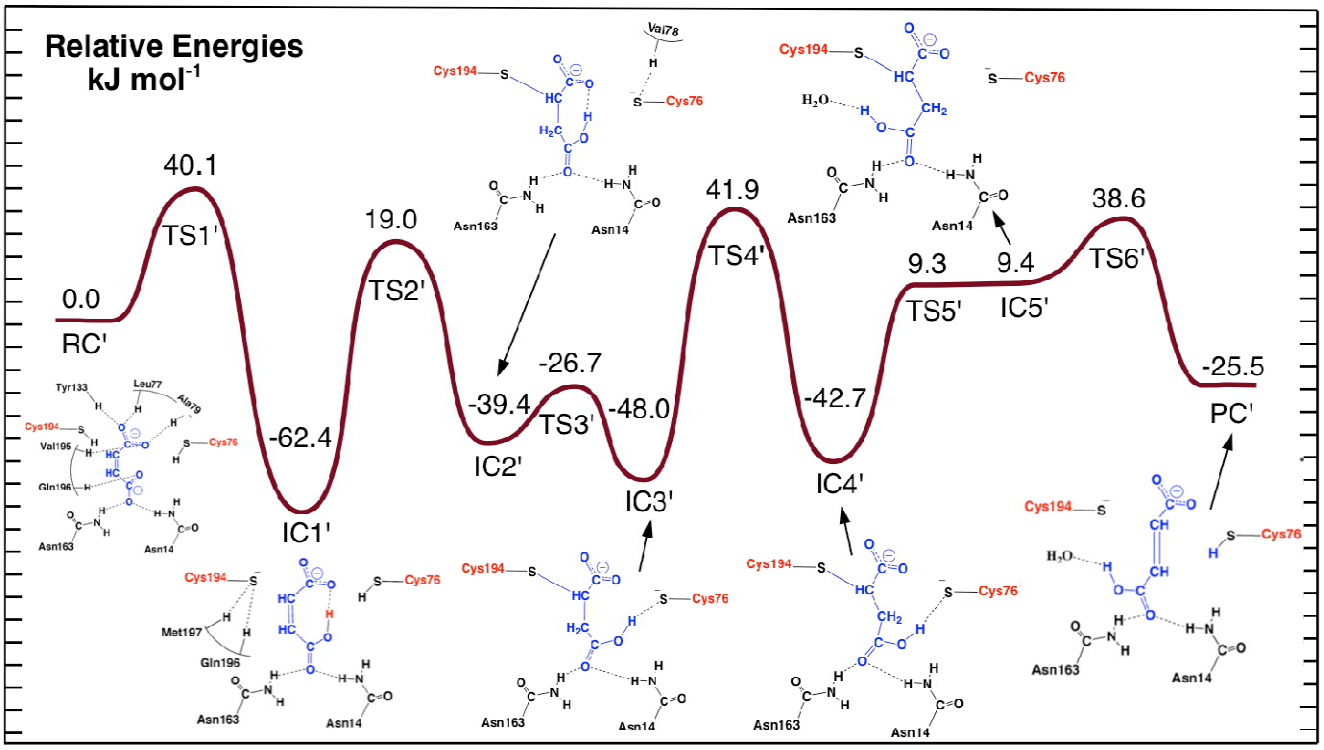

Figure 5 PES obtained using an ONIOM(QM/MM) approach (see Computational Methods) of the catalytic mechanism of MI in which Cys194 acts as a nucleophile.

Cys194-pathway: mechanism with Cys194 as the nucleophile

As noted above, the PA calculations suggested that rather than Cys76, Cys194 may in fact be preferably ionized within the substrate-bound active site. Hence, possible catalytic mechanisms in which Cys194 may act as the nucleophile were investigated. The resulting PES obtained is shown in Figure 5 while the corresponding optimized stationary point structures are illustrated in Scheme 8.

Beginning from the same **RC** as for the above mechanism in which Cys76 acts as the nucleophile, the first step is the analogous substrate facilitated activation of Cys194. This step, however, proceeds via **TS1'** at a cost relative to RC of only 40.1 kJ mol^{-1} (Figure 5). This is half that required to activate Cys76 via an analogous pathway (cf. Figure 4). Furthermore, unlike that observed for activation of Cys76, the Cys194 thiol proton is transferred directly onto an oxygen of the -C4OO$^-$ group with *r*(Cys194S···H) and *r*(H···OOC4) distances in **TS1'** of 1.63 and 1.24 Å, respectively (Scheme 7). The resulting intermediate formed **IC1'**, lies lower in energy than **RC** by 62.4 kJ mol^{-1}. Notably, this is 53.3 kJ mol^{-1} lower in energy than **IC1** on the Cys76-pathway (cf. Figure 4). This is likely due in part to the fact that in contrast to the single weak stabilizing hydrogen bond observed in **IC1**, in **IC1'** the Cys194S$^-$ thiolate forms three hydrogen bonds. Specifically, it forms two with the backbone –NH–'s of Gln196 and Met197, and one with the amide side chain of Asn163 via a water molecule. Meanwhile, as in **IC1**, the proton from Cys194 is wholly transferred onto the substrate's –C4OO$^-$ group and now forms an intermolecular hydrogen bond with the –C1OO$^-$ moiety. Also, the C2–C3 bond in **IC1'** (1.35 Å) remains little changed from that obtained for **RC**, in contrast to that observed for **IC1** in the alternate Cys76-pathway.

As for the Cys76-pathway the subsequent step is formation of a succinyl-Cys type intermediate (**IC2'**). Again this involves nucleophilic attack of the thiolate, though now it is Cys194S$^-$, at the substrates C2 center, with concomitant transfer of the thiol proton from the second active site cysteine (now Cys76) onto the adjacent C3 center. No stable enediolate intermediate could be found. This step occurs via **TS2'** with a barrier of 19.0 kJ mol^{-1} with respect to **RC**, or 81.4 kJ mol^{-1} relative to **IC1'**. The resulting succinyl-Cys intermediate **IC2'** lies lower in energy than **RC** by -39.4 kJ mol^{-1}. However, notably, this is in fact 52.1 kJ mol^{-1} *higher* in relative energy than the same corresponding intermediate **IC2** of the Cys76-pathway (cf. Figure 4). The C2–C3 bond has now elongated to 1.55 Å; that is, it is now a single bond.

At the heart of the isomerization mechanism is rotation about the C2—C3 bond, i.e., the *cis-trans* isomerization. In contrast to the seemingly one-step isomerization upon formation of a succinyl-Cys intermediate for the Cys76-pathway, a multi-step process was obtained on the Cys194-pathway (Figure 5). This process itself can be thought to occur in 3-stages. In the first, the intramolecular -C4OOH···$^-$OOC1- hydrogen bond is broken. Instead, the -C4OOH group now forms a strong hydrogen bond with the thiolate of Cys76S$^-$; *r*(C4OOH···$^-$SCys76) = 1.84 Å. This step occurs via **TS3'** with a low barrier of just 12.7 kJ mol^{-1} to give the alternate succinyl-Cys type intermediate **IC3'**. The latter in fact lies slightly lower in energy than **IC2'** by 8.6 kJ mol$^-$

[1]. More importantly, the ∠C2-C3-C4-O increases from 44.8° to 71.8°. Notably, the twist about the C2—C3 bond, i.e., ∠C1-C2-C3-C4 (ϕ), has slightly changed from that observed in **IC2'**, -294.3° to 306.0° in **IC3'**.

The next step is essentially the twist from a cis conformation to trans. This occurs via **TS4'** with a barrier of 41.9 kJ mol^{-1} relative to **RC** or 89.9 kJ mol^{-1} with respect to **IC3'**. In the resulting alternate succinyl-Cys type intermediate **IC4'**, lying just slightly higher in energy than **IC3'** by 5.3 kJ mol^{-1}, ∠C1-C2-C3-C4 (ϕ), has increased significantly to 137.2°. All active site-substrate interactions observed for **IC3'** are maintained (and the C2–C3 bond length stays the same as in **IC3'**). Importantly, this represents the rate-limiting step along the Cys194-pathway having both the highest barrier for a single reaction step and relative to **RC**. Furthermore, it is in good agreement with the barrier of ~70 kJ mol^{-1} calculated using experimental kinetics measurements.[34] In addition, it is significantly lower than the 135.1 kJ mol^{-1} required for the rate-limiting step of the alternate Cys76-pathway: going from **IC2** to **PC**.

The third stage is cleavage of the Cys76S$^-$···HOOC4 hydrogen bond. This step occurs via **TS5'** at a cost of 52.0 kJ mol^{-1} with respect to **IC4'**, or 9.3 kJ mol^{-1} relative to **RC**. In the resulting alternate succinyl-Cys type intermediate formed, **IC5'**, the C2–C3 bond has shortened by 0.02 Å to 1.53 Å, while the dihedral angle ∠C1-C2-C3-C4 is now 160.4°. More importantly, the C4OH group now forms a quite strong hydrogen bond of length 1.80 Å with an active site water molecule (Scheme 8). It should be noted that this latter water simultaneously forms a weak hydrogen bond (2.45 Å) with the sulfur of Cys194 (Scheme 8). In addition, the distance between the thiolate sulfur of Cys76 and the nearest -C3H$_2$- proton has now decreased from 3.05 Å in **IC4'** to 2.45 Å in **IC5'**. Thus, the Cys76 now seems well-positioned relative to the substrate to abstract a proton. Thermodynamically, **IC5'** has an energy relative to **RC** of 9.4 kJ mol^{-1}, 0.1 kJ mol^{-1} above that of **TS5'**. This is a common artefact of single-point energy calculations on a flat PES and indicates that the reverse reaction, **IC5'** to **IC4'**, essentially occurs without a barrier.

The final step is proton abstraction by the thiolate of Cys76 from the substrates -C3H2- moiety, with concomitant cleavage of the Cys194S—C2 bond. However, unlike the Cys76-pathway where the analogous step occurred with a high barrier, on the Cys194-pathway this step proceeds via **TS6'** at a very low cost of only 29.9 kJ mol^{-1} relative to **IC5'**. The concerted nature of this step is highlighted by the fact that in **TS6'** the Cys194S···C2 bond has elongated to 1.97 Å, while the C3H···SCys76 and C3—HSCys76 distances are now 1.65 and 1.50 Å, respectively. The final product complex **PC**, in which fumarate is now non-covalently bound within the active site, is 25.5 kJ mol^{-1} lower in energy than **RC** with a C2–C3 bond of 1.35 Å. Thus, unlike that calculated above for the Cys76-pathway, this alternate mechanism in which Cys194 acts as the nucleophile is thermodynamically favoured.

Conclusions

In this study the mechanism by which the enzyme maleate isomerase catalyzes the cis-trans interconversion of maleate and fumarate has been computationally investigated. Specifically, DFT methods in combination with small chemical models were used to gain fundamental insights into the nature of possible mechanistic intermediates, while QM-cluster and ONIOM(QM/MM) methods have been used to examine the nature of the substrate-bound active site and the catalytic mechanism.

The feasibility of the formation of proposed enediolate and succinyl-Cys type intermediates from a neutral, monoanionic or dianionic maleate substrate was initially examined using DFT-small chemical model studies For both neutral and monoanionic maleate an enediolate intermediate, formed by nucleophilic attack of methyl thiolate (CH_3S^-) at their C2 center, was unstable, i.e., dissociated back to the original substrates. In contrast, the succinyl-Cys type intermediate, formed by concomitant thiolate addition to C2 and protonation of C3, was stable for all 3 ionization states of the initial maleate. Furthermore, for dianionic maleate the formation of succinyl-Cys leads to a barrierless rotation about the substrates central C2—C3 bond. Increasing the polarization of the environment was observed to decrease the angle of rotation. In order to understand the driving force for rotation, the LUMO and HOMO were also examined.

The ionization state of the active site cysteinyl's (Cys76 and Cys194) and the substrate were examined using an ONIOM(QM/MM) based approach for both the apoenzyme and the substrate-bound active site. The results suggest that the proton affinity (PA) of Cys76S$^-$ is higher than that of Cys194S$^-$ in both the apo-enzyme and when the dianionic maleate substrate is bound within the active. Furthermore, the combined results suggest that upon substrate binding the preferred initial state of the substrate-bound active site contains a monoanionic maleate substrate, an ionized Cys194 (i.e., Cys194S$^-$) and a neutral Cys76 (i.e., Cys76SH).

Two possible mechanistic pathways were investigated using QM-cluster and/or an ONIOM(QM/MM) approach. The first pathway corresponds to that previously experimentally proposed in which the active site residue Cys76 acts as the mechanistic nucleophile that attacks the substrates sp^2 C2 centre; the Cys76-pathway. In the alternate pathway Cys194 acts as the required nucleophile; the Cys194-pathway.

In both pathways the Cys76 or Cys194 thiol, can be deprotonated via proton transfer onto the maleate substrate's carboxylate positioned nearest Asn14 and Asn163. However, the barrier for this step on the Cys194-pathway (40.1 kJ mol^{-1}) is only half that of the analagous step on the Cys76-pathway (80.2 kJ mol^{-1}). This is due in part to greater stabilization of Cys194S$^-$ than Cys76S$^-$ by hydrogen bonding within the active site.

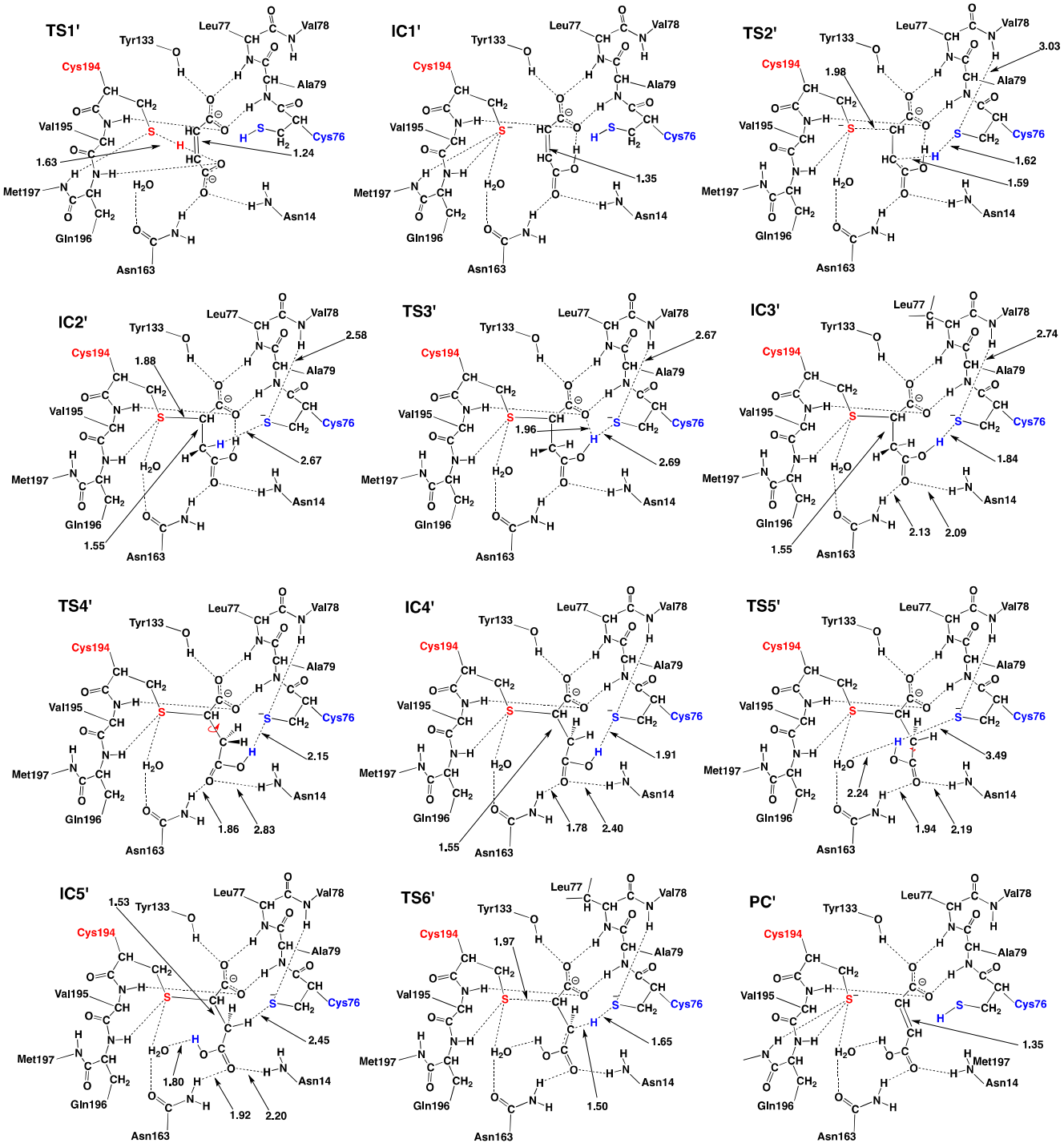

Scheme 8 Schematic illustration of optimized structures obtained using an ONIOM(QM/MM) approach (see Computational Methods) for the mechanism in which Cys194 acts as nucleophile.

The subsequent step in these pathways is the nucleophilic attack of the thiolate at the maleate substrate's C2 centre. Additionally, this occurs with concomitant proton transfer from the R-group thiol of the second active site cysteinyl to give a succinyl-Cys intermediate (**IC2** and **IC2'**, respectively). Importantly, in the case of the Cys76-pathway such an intermediate (**IC2**) lies significantly lower in energy than the initial reactant complex (**RC**) by 91.5 kJ mol^{-1}. Furthermore, subsequent rearrangement and reaction of **IC2** to give the final product complex (**PC**) requires a considerable amount of energy; 135.1 kJ mol^{-1}. This is in fact the rate-limiting process of the Cys76-pathway. In contrast, for the Cys194-pathway the resulting succinyl-Cys intermediate (**IC2'**), while lower in energy than the **RC**, is not as significantly stabilized, lying just 39.4 kJ mol^{-1} lower in energy than **RC**. It is able to undergo a series of relatively low-energy rearrangements and reactions to give the final product complex (**PC'**). The rate-limiting step along the Cys194-pathway is the step in which a twist from a cis

conformation to trans occurs. The calculated barrier for this step if 89.9 kJ mol^{-1} is in good agreement with the barrier calculated using experimentally determined kinetics; ~70 kJ mol^{-1}.[34]

Thus, the present results suggest that the overall catalytic mechanism of Maleate Isomerase is initiated by a substrate-assisted activation of the active site cysteinyl Cys194. This is followed by the concerted formation of a succinyl-Cys intermediate in which Cys76 acts as an acid. Thus, Cys194 is the mechanistic nucleophile while Cys76 instead acts as an acid/base along the mechanism. The desired rotation about the C2—C3 bond occur via multiple relatively low-barrier steps with assistance of the anionic Cys76S–, generated during formation of a succinyl-Cys intermediate. Finally, cleavage of the Cys194S–C2 bond concomitant with proton abstraction by $Cys76S^{-}$ from the intermediates C3H2 group leads to the formation of the fumarate product. The conserved nature of the active site in the racemase superfamily suggests possible transferability of the mechanism outlined to other species in the family.

ACKNOWLEDGMENT

We thank the Natural Sciences and Engineering Research Council of Canada (NSERC) for funding and Compute Canada for additional computational resources, and the Ontario Graduate Scholarship program (B.F.I.) for financial support.

Notes and references

Department of Chemistry and Biochemistry, University of Windsor, Windsor, Ontario, N9B 3P4, Canada. Fax: +1 5199737089; Tel: +1 5192533000 Ext:3992; E-Mail: gauld@uwindsor.ca

† Electronic Supplementary Information (ESI) available: [energies and optimized structures]. See DOI: 10.1039/b000000x/

‡ Footnotes should appear here. These might include comments relevant to but not central to the matter under discussion, limited experimental and spectral data, and crystallographic data.

1. J. A. Prescher and C. R. Bertozzi, *Nat. Chem. Biol.*, 2005, **1**, 13-21.
2. G. Fischer, in *Cis-Trans isomerization in biochemistry*, ed. C. Dugave, Wiley-VCH Verlag GmbH & Co. KGaA, Weinheim, Germany, 2006.
3. E. Hrabovszky and Z. Liposits, *J. Neuroendocrinol.*, 2008, **20**, 743-751.
4. E. Mixcoha,M. Garcia-Viloca,J. M. Lluch and A. Gonzalez-Lafont, *J. Phys. Chem. B*, 2012, **116**, 12406-12414.
5. C. B. Trapnell, *AIDS clinical care*, 1998, **10**, 3, 8.
6. S. Fabro,R. L. Smith and R. T. Williams, *Nature*, 1967, **215**, 296-&.
7. C. Dugave, in *Cis-Trans isomerization in biochemistry*, ed. C. Dugave, Wiley-VCH Verlag GmbH & Co. KGaA, Weinheim, Germany, 2006.
8. Y. Koyama,Y. Kakitani and H. Nagae, in *Cis-Trans isomerization in biochemistry*, ed. C. Dugave, Wiley-VCH Verlag GmbH & Co. KGaA, Weinheim, Germany, 2006.
9. F. A. Fisch, University of York, 2009.
10. L. X. Wang,C. H. Yi,H. T. Zou,J. Xu and W. L. Xu, *J. Phys. Org. Chem.*, 2009, **22**, 888-896.
11. D. P. Hoffman and R. A. Mathies, *Phys. Chem. Chem. Phys.*, 2012, **14**, 6298-6306.
12. K. Mizuno,K. Nire,H. Sugita and H. Maeda, *Tetrahedron Lett.*, 2001, **42**, 2689-2692.
13. G. Polekhina,P. G. Board,A. C. Blackburn and M. W. Parker, *Biochemistry*, 2001, **40**, 1567-1576.
14. M. Marsh,D. K. Shoemark,A. Jacob,C. Robinson,B. Cahill,N. Y. Zhou,P. A. Williams and A. T. Hadfield, *J. Mol. Biol.*, 2008, **384**, 165-177.
15. T. M. Redmond,E. Poliakov,S. Kuo,P. Chander and S. Gentleman, *J. Biol. Chem.*, 2010, **285**, 1919-1927.
16. J. Fanghanel and G. Fischer, *Front. Biosci.*, 2004, **9**, 3453-3478.
17. P. K. Agarwal, *Proteins*, 2004, **56**, 449-463.
18. E. Puig,M. Garcia-Viloca,A. Gonzalez-Lafont,J. M. Lluch and M. J. Field, *J. Phys. Chem. B*, 2007, **111**, 2385-2397.
19. T. Lundqvist,S. L. Fisher,G. Kern,R. H. A. Folmer,Y. F. Xue,D. T. Newton,T. A. Keating,R. A. Alm and B. L. M. de Jonge, *Nature*, 2007, **447**, 817-822.
20. K. Hatakeyama,M. Goto,Y. Uchida,M. Kobayashi,M. Terasawa and H. Yukawa, *Biosci. Biotechnol. Biochem.*, 2000, **64**, 569-576.
21. E. Puig,E. Mixcoha,M. Garcia-Viloca,A. Gonzalez-Lafont and J. M. Lluch, *J. Am. Chem. Soc.*, 2009, **131**, 3509-3521.
22. K. Okrasa,C. Levy,B. Hauer,N. Baudendistel,D. Leys and J. Micklefield, *Chem.-Eur. J.*, 2008, **14**, 6609-6613.
23. B. L. M. de Jonge,A. Kutschke,M. Uria-Nickelsen,H. D. Kamp and S. D. Mills, *Antimicrob. Agents Chemother.*, 2009, **53**, 3331-3336.
24. A. Zeida,C. Guardia,P. Lichtig,L. Perissinotti,L. Defelipe,A. Turjanski,R. Radi,M. Trujillo and D. Estrin, *Biophys Rev*, 2014, 1-20.
25. W. Scher and W. B. Jakoby, *J. Biol. Chem.*, 1969, **244**, 1878-1882.
26. K. Hatakeyama,Y. Asai,Y. Uchida,M. Kobayashi,M. Terasawa and H. Yukawa, *Biochem. Biophys. Res. Commun.*, 1997, **239**, 74-79.
27. K. Tanaka,K. Kobayashi and N. Ogasawara, *Microbiology-(UK)*, 2003, **149**, 2317-2329.
28. Y. Kato,J. Yamagishi and Y. Asano, *J. Ferment. Bioeng.*, 1995, **80**, 610-612.
29. C. A. R. Engel,A. J. J. Straathof,T. W. Zijlmans,W. M. van Gulik and L. A. M. van der Wielen, *Appl. Microbiol. Biotechnol.*, 2008, **78**, 379-389.
30. D. D. Chen,H. Z. Tang,Y. Lv,Z. Y. Zhang,K. L. Shen,K. Lin,Y. L. Zhao,G. Wu and P. Xu, *Molecular Microbiology*, 2013, **87**, 1237-1244.
31. T. D. H. Bugg,D. Braddick,C. G. Dowson and D. I. Roper, *Trends Biotechnol.*, 2011, **29**, 167-173.
32. S. Ichikawa,T. Iino,S. Sato,T. Nakahara and S. Mukataka, *Biochem. Eng. J.*, 2003, **13**, 7-13.
33. Y. Takamura,T. Takamura,M. Soejima and T. Uemura, *Agric. Biol. Chem.*, 1969, **33**, 718-728.
34. F. Fisch,C. M. Fleites,M. Delenne,N. Baudendistel,B. Hauer,J. P. Turkenburg,S. Hart,N. C. Bruce and G. Grogan, *J. Am. Chem. Soc.*, 2010, **132**, 11455-11457.
35. R. Obata and M. Nakasako, *Biochemistry*, 2010, **49**, 1963-1969.
36. T. Borowski,V. Georgiev and P. Siegbahn, *J. Mol. Model*, 2010, **16**, 1673-1677.
37. M. Stenta,M. Calvaresi,P. Altoe,D. Spinelli,M. Garavelli,R. Galeazzi and A. Bottoni, *J. Chem. Theory Comput.*, 2009, **5**, 1915-1930.
38. R.-Z. Liao,F. Himo,J.-G. Yu and R.-Z. Liu, *Journal of Inorganic Biochemistry*, 2010, **104**, 37-46.
39. J. G. Llano, J. W. , in *Quantum Biochemistry: Electronic Structure and Biological ActiVity*, ed. C. F. Matta, Ed.; , Wiley-VCH: Weinheim, 2010, vol. 2, p. 643.

40. MOE., (2009) Chemical Computing Group Inc, Montreal, Quebec, Canada.
41. M. J. Frisch,G. W. Trucks,H. B. Schlegel,G. E. Scuseria,M. A. Robb,J. R. Cheeseman,J. A. J. Montgomery,T. Vreven,K. N. Kudin,J. C. Burant,J. M. Millam,S. S. Iyengar,J. Tomasi,V. Barone,B. Mennucci,M. Cossi,G. Scalmani,N. Rega,G. A. Petersson,H. Nakatsuji,M. Hada,M. Ehara,K. Toyota,R. Fukuda,J. Hasegawa,M. Ishida,T. Nakajima,Y. Honda,O. Kitao,H. Nakai,M. Klene,X. Li,J. E. Knox,H. P. Hratchian,J. B. Cross,C. Adamo,J. Jaramillo,R. Gomperts,R. E. Stratmann,O. Yazyev,A. J. Austin,R. Cammi,C. Pomelli,J. Ochterski,P. Y. Ayala,K. Morokuma,G. A. Voth,P. Salvador,J. J. Dannenberg,V. G. Zakrzewski,S. Dapprich,A. D. Daniels,M. C. Strain,O. Farkas,D. K. Malick,A. D. Rabuck,K. Raghavachari,J. B. Foresman,J. V. Ortiz,Q. Cui,A. G. Baboul,S. Clifford,J. Cioslowski,B. B. Stefanov,G. Liu,A. Liashenko,P. Piskorz,I. Komaromi,R. L. Martin,D. J. Fox,T. A. Keith,M. A. Al-Laham,C. Y. Peng,A. Nanayakkara,M. Challacombe,P. M. W. Gill,B. G. Johnson,W. Chen,M. W. Wong,C. Gonzalez and J. A. Pople, *Gaussian 03*, (2004) Gaussian Inc., Wallingford CT.
42. R. A. Gaussian 09, M. J. Frisch, G. W. Trucks, H. B. Schlegel, G. E. Scuseria, M. A. Robb, J. R. Cheeseman, G. Scalmani, V. Barone, B. Mennucci, G. A. Petersson, H. Nakatsuji, M. Caricato, X. Li, H. P. Hratchian, A. F. Izmaylov, J. Bloino, G. Zheng, J. L. Sonnenberg, M. Hada, M. Ehara, K. Toyota, R. Fukuda, J. Hasegawa, M. Ishida, T. Nakajima, Y. Honda, O. Kitao, H. Nakai, T. Vreven, J. A. Montgomery, Jr., J. E. Peralta, F. Ogliaro, M. Bearpark, J. J. Heyd, E. Brothers, K. N. Kudin, V. N. Staroverov, R. Kobayashi, J. Normand, K. Raghavachari, A. Rendell, J. C. Burant, S. S. Iyengar, J. Tomasi, M. Cossi, N. Rega, J. M. Millam, M. Klene, J. E. Knox, J. B. Cross, V. Bakken, C. Adamo, J. Jaramillo, R. Gomperts, R. E. Stratmann, O. Yazyev, A. J. Austin, R. Cammi, C. Pomelli, J. W. Ochterski, R. L. Martin, K. Morokuma, V. G. Zakrzewski, G. A. Voth, P. Salvador, J. J. Dannenberg, S. Dapprich, A. D. Daniels, Ö. Farkas, J. B. Foresman, J. V. Ortiz, J. Cioslowski, and D. J. Fox, Gaussian, Inc., Wallingford CT, 2009.
43. A. D. Becke, *J. Chem. Phys.*, 1993, **98**, 1372-1377.
44. C. Lee,W. Yang and R. G. Parr, *Phys. Rev. B*, 1988, **37**, 785-789.
45. P. E. M. Siegbahn and M. R. A. Blomberg, *Chem. Rev.*, 2000, **100**, 421 - 437.
46. L. Noodleman,T. Lovell,W.-G. Han,J. Li and F. Himo, *Chem. Rev.*, 2004, **104**, 459-508.
47. E. A. C. Bushnell,E. Erdtman,J. Llano,L. A. Eriksson and J. W. Gauld, *J. Comput. Chem.*, 2010, **32**, 822-834.
48. E. A. C. Bushnell,W. Huang,J. Llano and J. W. Gauld, *J. Phys. Chem. B*, 2012, **116**, 5205-5212.
49. J. M. Wang,R. M. Wolf,J. W. Caldwell,P. A. Kollman and D. A. Case, *J. Comput. Chem.*, 2004, **25**, 1157-1174.
50. S. F. Sousa,P. A. Fernandes and M. J. Ramos, *Phys. Chem. Chem. Phys.*, 2012, **14**, 12431-12441.
51. M. Svensson,S. Humbel,R. D. J. Froese,T. Matsubara,S. Sieber and K. Morokuma, *J. Phys. Chem.*, 1996, **100**, 19357-19363.
52. J. L. Przybylski and S. D. Wetmore, *Biochemistry*, 2011, **50**, 4218-4227.
53. I. Razmisleviciene,R. Baltuskonyte,A. Padarauskas and E. Naujalis, *Chemija*, 2008, **19**, 33-37.
54. V. I. Lim,J. F. Curran and M. B. Garber, *J. Mol. Biol.*, 2005, **351**, 470-480.
55. V. I. Lim and V. G. Kljashtorny, *Mol. Biol.*, 2006, **40**, 572-579.